Coupled Reservoir-Geomechanical Analysis of the Potential for Tensile and Shear Failure Associated with CO_2 Injection in Multilayered Reservoir-Caprock Systems

J. Rutqvist*, J.T. Birkholzer, and Chin-Fu Tsang

Lawrence Berkeley National Laboratory, Earth Sciences Division, MS 90-1116, Berkeley, CA 947 20, USA

* Corresponding author. Tel.: +1-510-486-5432, fax.: +1-510-486-5686
E-mail address: Jrutqvist@lbl.gov (J. Rutqvist)

ABSTRACT

Coupled reservoir-geomechanical simulations were conducted to study the potential for tensile and shear failure—e.g., tensile fracturing and shear slip along pre-existing fractures—associated with underground CO_2 injection in a multilayered geological system. This failure analysis aimed to study factors affecting the potential for breaching a geological CO_2 storage system and to study methods for estimating the maximum CO_2 injection pressure that could be sustained without causing such a breach. We pay special attention to geomechanical stress changes resulting from upward migration of the CO_2 and how the initial stress regime affects the potential for inducing failure. We conclude that it is essential to have an accurate estimate of the three-dimensional *in situ* stress field to support the design and performance assessment of a geological CO_2 injection operation. Moreover, we also conclude that it is important to consider mechanical stress changes that might occur outside the region of increased reservoir fluid pressure (e.g., in the overburden rock) between the CO_2-injection reservoir and the ground surface.

1 INTRODUCTION

Deep underground injection of carbon dioxide (CO_2) has emerged in recent years as an important option for sequestering CO_2 and thereby reducing the emission of greenhouse gases to the atmosphere. Because CO_2 is less dense than water, the targeted CO_2 injection reservoir should be overlain by low-permeability caprock formations that can sufficiently limit upward buoyancy-driven flow of the injected CO_2. However, caprock layers may be discontinuous and heterogeneous, and may contain imperfections—such as faults or fracture zones—that could provide permeable conduits for CO_2 migration towards the near-surface environment. Furthermore, increasing reservoir pressure in response to CO_2 injection induces mechanical stresses and deformations in and around the injection reservoir. If reservoir pressure becomes too large, the induced stresses may cause irreversible mechanical changes, creating new fractures or reactivating old ones. Such changes could open new flow paths through otherwise low-permeability capping formations, thereby substantially reducing the effectiveness of sequestration.

In predicting the performance of a particular site for CO_2 sequestration, much can be learned from studies related to the geological containment of gases in naturally overpressured sediments and gas reservoirs [1, 2]. In such formations, initiation and reactivation of brittle faults and fractures within low-permeability capping formations limit the degree of natural overpressure. Sibson [2] concludes that re-shear of existing cohesionless faults and fractures favorably oriented for frictional reactivation provides the lower bound to overpressures, whereas drainage of conduits by hydraulic extension fracturing is important only in the case of intact caprock under low differential stress.

Moreover, the maximum overpressure that can be sustained is strongly dependent on the *in situ* stress regime, including the difference in the magnitudes of maximum and minimum principal stress. Rutqvist and Tsang [3] found analogous results in a coupled reservoir-geomechanical simulation of CO_2 injection into a reservoir capped by a single caprock unit: in an extensional stress regime ($S_H = 0.7S_v$), reactivation of steeply dipping fractures is most likely to occur, whereas in a compressional stress regime ($S_h = 1.5S_v$), reactivation of shallowly dipping fractures is most likely, but at a higher injection pressure. Given the role of fault reactivation and fracturing in naturally overpressured reservoirs, shear and tensile failure analysis is essential for the design and performance assessment of geological CO_2 sequestration sites.

Analysis of tensile and shear failure can be conducted using simplified analytical techniques as well as using more complex numerical techniques. Analytical techniques were originally developed and applied to study earthquakes as well as the effects of fault reactivation on hydrocarbon accumulations, but have also been used to evaluate fault stability associated with CO_2 sequestration (e.g., [4]). These techniques are commonly based on estimated regional *in situ* principal stress magnitudes and orientations with respect to pre-existing fault planes, assuming a cohesionless fault surface [5, 6, 7, 8]. Such simplified analytical techniques are very useful for a first-order estimate of the maximum sustainable CO_2 injection pressure, and for identification of the most critically oriented faults in the system. However, coupled reservoir-geomechanical numerical simulations have shown that the *in situ* stress field does not remain constant during underground CO_2 injections, but rather evolves over time and space, controlled by the

evolution of fluid pressure in the system and the site-specific structural geometry [3, 9]. Although analytical techniques can be used to estimate such stress changes in general, a coupled reservoir-geomechanical analysis might be used for a more detailed analysis of heterogeneous stress changes occurring within and around the injection zone.

In this paper, we present the results from coupled reservoir-geomechanical simulations to gauge the potential for tensile and shear failure caused by CO_2 injection. The simulations were performed using the coupled reservoir-geomechanical simulator TOUGH-FLAC, which is described in detail by Rutqvist et al. [10], and Rutqvist and Tsang [11]. This study extends previous simulation studies on single caprock systems [3, 9] to multilayered and faulted systems in which CO_2 and fluid pressure can migrate upwards into overlying formations (Figure 1). A multilayered rather than a single caprock system is a viable option for geological storage of CO_2, because multiple caprocks, though not completely impermeable, can divert and delay upward migration of CO_2. The multilayered system considered here is different from that of the Utsira Formation at the Sleipner gas field in the North Sea, where CO_2 has been injected since 1996 [12]. At the Sleipner's Utsira Formation, seismic profiling of the CO_2 plume has suggested upward migration of CO_2 around thin intrareservoir shales, whereas in this example, the upward migration takes place through permeable damaged zones across thicker shale layers.

In this study, we analyze mechanical stress changes and the potential for mechanical failure associated with the upward migration of the CO_2, including associated buoyancy effects on the pressure column in relation to the depth-dependent *in situ* stress field. The

potential for tensile and shear failure is calculated, based on the time-dependent evolution and local distribution of fluid pressure and the three-dimensional stress field, accounting for poroelastic stresses. We pay special attention to the impact of the *in situ* stress regimes, whether isotropic, compressional, or extensional stress regimes. Finally, based on a comparison of our numerical results to those of simplified analytical methods, we discuss possible guidelines for estimating maximum sustainable injection pressure at a geological CO_2 injection site.

2 MODEL SETUP OF THE GEOLOGICAL CO_2 STORAGE SYSTEM

In this study, CO_2 is injected into a CO_2-storage system that consists of several layers of permeable brine-water formations, interlaced with layers of low-permeability caprock formations (Figure 1). The system is represented in a two-dimensional plane-strain model that extends vertically from the ground surface to a depth of 3,000 m, and horizontally six hundred kilometers to simulate laterally infinite acting conditions. At the bottom and lateral boundaries, pressure, temperature and normal displacements are fixed (Figure 1). Initial conditions include a hydrostatic pressure gradient and a temperature gradient defined as T = 10.0-0.025z, where z is the elevation. Moreover, a depth-dependent three-dimensional initial stress field is defined, depending on which stress regime is considered. The applied stress field for each assumed stress regime is described in detail in Section 4.

The injection is conducted at 1,600 m depth (z = -1,600 m) in a 200 m thick brine formation (Injection Zone 1 in Figure 1). The injection zone is hydraulically connected to overlying reservoir Zones 2 and 3 through permeable vertical connections across Caprocks 1 and 2, envisioned as zones of damaged and highly fractured rocks along a major fault. These permeable vertical connections provide limited upward migration of CO_2 from the injection zone into the upper formations of the CO_2-storage system. However, the vertical fractured zone is not continuously permeable through Caprock 3, which should provide the ultimate protection against upward leakage to the near-surface environment. Thus, in this analysis it is important to study the geomechanical effects in Caprock 3, and whether its sealing capacity will remain intact, even in the case of pre-existing breaches in Caprocks 1 and 2.

Hydraulic and mechanical formation properties are given in Table 1, with the properties for the permeable formations and the caprocks representing sandstone and shale, respectively. The simulation is conducted in isothermal mode, although the fixed temperature gradient affects temperature-dependent fluid properties. Relative permeability of gas and liquid phases was calculated from Corey's function [13], while capillary pressure was governed by the van Genuchten function [14]. The multiphase fluid-flow simulation was conducted with the newly developed fluid property module ECO2N [15], which contains a comprehensive description of the thermodynamic and thermophysical properties of water-NaCl-CO_2 mixtures needed for analysis of CO_2 sequestration in brine-saturated formations.

The analysis was conducted in two steps: (1) a basic coupled reservoir-geomechanical analysis to calculate injection-induced changes in the stress field, and (2) a failure analysis using the stress field calculated in Step 1. The basic reservoir-geomechanical analysis was conducted with a linear poroelastic model, using mechanical properties given in Table 1. For simplicity, the elastic properties were assumed to be the same for all formations, except for the fractured rock zone through Caprocks 1 and 2, where a reduction of 50% in Young's modulus was assumed to represent the effect of increased fracturing. Note that although we are using a two-dimensional plane strain model, we are able to calculate changes in the three-dimensional stress field, including stresses within the x-z plane as well as out-of-plane stress (i.e., stress in the y-direction).

3 COUPLED RESERVOIR-GEOMECHANICAL SIMULATION

In this simulation, we inject CO_2 at a constant rate of 0.04 kg/m/s for 30 years, which represents a reasonable injection rate produced from a single coal-fired power plant [9]. The CO_2 is injected as supercritical fluid and forms a CO_2-rich fluid phase that displaces the native brine within the CO_2 storage system. The CO_2 spreads both laterally and upward across Caprocks 1 and 2, as significant flow is allowed through the fractured rock zones (Figure 2a). During the 30-year injection period, reservoir pressure increases gradually. At the end of the 30-year injection period, the downhole pressure has increased by 9 MPa, from 16 to 25 MPa, which is well below the lithostatic stress of about 35 MPa at the depth of the injection zone.

The poroelastic modeling shows that effective stress decreases as fluid pressure increases within the CO_2-storage system (Figure 2b). In general, changes of vertical and horizontal effective stresses within the x-z plane of our model, $\Delta\sigma'_z$ and $\Delta\sigma'_x$, are a function of changes in fluid pressure, ΔP, and changes in total vertical and horizontal stresses, $\Delta\sigma_z$ and $\Delta\sigma_x$, according to:

$$\Delta\sigma'_z = \Delta\sigma_z - \alpha\Delta P \quad (1)$$

$$\Delta\sigma'_x = \Delta\sigma_x - \alpha\Delta P \quad (2)$$

with the convention of compressive stresses being positive. In Equations (1) and (2), α is the Biot's coefficient, which in this case was taken to be 1 (Table 1).

Figure 2 shows that decreases in vertical effective stress correspond to increases in fluid pressure—that is, $\Delta\sigma'_z \approx -\Delta P$ at every point (compare solid contour lines in Figure 2b with dashed contour lines in Figure 2a). The resulting $\Delta\sigma'_z \approx -\Delta P$ implies that changes in the total stress component in Equation (2) must be close to zero—that is, $\Delta\sigma_z \approx 0$. Figure 2b shows that the decrease in horizontal effective stress is much smaller than the decrease in vertical effective stress. Furthermore, the decrease in horizontal effective stress is smaller than the increase in fluid pressure, which according to Equation (2) shows that the total horizontal stress must increase. For example, around the injection point, $\Delta P \approx 9$ MPa, while $\Delta\sigma'_x \approx -5$ MPa (Figure 2). Then, according to Equation (1), $\Delta\sigma_x = \Delta\sigma'_x + \Delta P = -5 + 9 = 4$ MPa; that is, the total horizontal compressive stress increases by 4 MPa as a result of the injection.

As will be further discussed in Section 4, the total *in situ* horizontal stress field increases within the pressurized zone as a result of poroelastic stressing in a laterally confined rock mass. The total vertical stresses, on the other hand, do not change significantly during the CO_2 injection, because the rock mass is free to expand in the vertical direction as a result of the free-moving ground surface and the large lateral extension of the pressurized zone.

In addition to changes in stresses within the x-z plane discussed above, there is also a significant change in out-of-plane horizontal effective stress (i.e. $\Delta\sigma'_y \neq 0$). The distribution of $\Delta\sigma'_y$ is similar distribution to that of $\Delta\sigma'_x$ shown in Figure 2b, but the magnitude is smaller. Under the assumed plane-strain conditions, the maximum change in out-of-plane effective stress, $\Delta\sigma'_y$ is about 3 MPa, and total stress, $\Delta\sigma_y$ is about 6 MPa.

4 ASSESSING THE LIKELIHOOD OF MECHANICAL FAILURE

After calculating the evolution of fluid pressure and the related changes in the three-dimensional poroelastic stress, we analyze the possibility of failure by studying the critical pressure that could induce tensile or shear failure along pre-existing fractures.

The potential for mechanical failure is analyzed for three types of stress regimes: an isotropic stress regime ($S_x = S_y = S_z$), and a compressional stress regime ($S_x = 1.5S_z$ and assuming $S_x = S_1$ and $S_z = S_3$), an extensional stress regime ($S_x = 0.7S_z$ and assuming $S_x = S_2$ and $S_z = S_1$). Note that S_x, S_y, S_z refer to x, y, and z components; and S_1, S_2, S_3 refer to principal components of the initial (pre-injection) three-dimensional stress field. Moreover, note that the extensional stress regime is equivalent to a normal faulting stress

regime, whereas a compressional stress regime could either be a reverse or strike-slip faulting stress regime. In this simulation study, the compressional stress regime refers to the particular case of a reverse faulting stress regime. In all cases, the initial vertical stress, S_z, is calculated from the weight of the overburden rock, assuming a rock density of 2,260 kg/m^3. The evolution of the three-dimensional stress field during CO_2 injection is obtained by superimposing the poroelastically induced stress distribution calculated in Section 3 on top of the assumed initial stress. That is, at each point, the correct stress is calculated as $\sigma_x = S_x + \Delta\sigma_x$, $\sigma_y = S_y + \Delta\sigma_y$, and $\sigma_z = S_z + \Delta\sigma_z$. The potential for failure is then calculated for each of the three *in situ* stress regimes.

In our calculations, we select the initial out-of-plane stress S_y to satisfy the conditions for isotropic, compressional, or extensional stress regimes. Moreover, for the compressional and extensional stress regimes, the out-of-plane stress is selected such that the injection-induced poroelastic stressing is not sufficient to rotate the principal stress field. This condition was satisfied in the case of compressional and extensional stress regimes by selecting out-of-plane stress S_y as being S_2, with a magnitude slightly higher than S_3. Thus, in the case of a compressional stress regime, S_y is slightly higher than S_z, whereas in the case of an extensional stress regime, S_y is slightly higher than S_x. For the isotropic case, S_y is set equal to S_x and S_z.

In this study, the potential for tensile failure is calculated using the conservative assumption that a tensile fracture could develop as soon as the fluid pressure exceeds the

least compressive principal stress, leading to a critical fluid pressure for fracturing (P_{fc}) according to:

$$P_{fc} = \sigma_3 \tag{3}$$

This could also include tensile reactivation of pre-existing fracture planes that might be filled and healed by minerals (e.g., calcite).

The potential for shear failure (or shear slip) along pre-existing fractures is calculated using the conservative assumption that a fracture could exist at any point with an arbitrary orientation. For such a case, the Coulomb failure criterion can be written in the following form [16]:

$$|\tau_{m2}| = (\sigma_{m2} - P_{sc})\sin\varphi + S_0\cos\varphi \tag{4}$$

where τ_{m2} and σ_{m2} are the two-dimensional maximum shear stress and mean stress in the plane σ_1, σ_3, defined as:

$$\tau_{m2} = \frac{1}{2}(\sigma_1 - \sigma_3) \tag{5}$$

$$\sigma_{m2} = \frac{1}{2}(\sigma_1 + \sigma_3) \tag{6}$$

with S_0 and φ the coefficient of internal cohesion and angle of internal friction, respectively, and P_{sc} the critical fluid pressure for the onset of shear failure.

As a lower limit for likely shear failure, zero cohesion may be assumed and a typical range for φ is 25° to 35° [17]. Thus, in this study, we test for shear failure (or slip) using

zero cohesion ($S_0 = 0$) and a friction angle of 30°, leading to the following critical fluid pressure for the onset of slip:

$$P_{sc} = \sigma_{m2} - 2|\tau_{m2}| \tag{7}$$

A friction angle of 30° corresponds to a static coefficient of friction $\mu_s = \tan 30° = 0.577 \approx 0.6$, which is a lower-limit value observed for hydraulically conductive fractures and their correlation with *in situ* stresses in fractured rock masses (e.g., [18]).

The potential for failure may be expressed in many ways (e.g., the ratio of the ambient shear stress on a fracture plane over its shear strength). However, in this study, we express the potential for failure (tensile or shear failure) in terms of a pressure margin for the onset of failure (according to Rutqvist and Tsang [9]). We define a pressure margin, P_{fm}, for the onset of tensile fracturing as

$$P_{fm} = P - P_{fc} = -\sigma'_3 \tag{8}$$

which should be negative to prevent fracturing. Thus, P_{fm} tells us how much further the fluid pressure can be increased before tensile failure is initiated. Similarly, we define a pressure margin, P_{sm}, for the onset of shear failure (or slip) [9] as

$$P_{sm} = P - P_{sc} = -\sigma'_{m2} + 2|\tau_{ms}| \tag{9}$$

which should be negative to prevent shear failure.

Figure 3 presents contours of pressure margins for onset of shear failure (Equation 9) under compressional and extensional stress regimes. In the figure, the only location of

high potential for tensile failure ($P_{fm} > 0$, determined by Equation 8) has also been indicated. This location is near the bottom of Caprock 3 in the case of an extensional stress regime (Figure 3b). A high potential for tensile failure exists only in the case of an extensional stress regime, because the initial minimum principal stress is the lowest in that case, being horizontal with a magnitude of $0.7\sigma_z$. However, the tensile failure would be very limited in extent, even for the unfavorable case of a low horizontal *in situ* stress.

The results in Figure 3 clearly illustrate the potential for injection-induced shear failure and its correlation to the initial stress regime. There is a high potential for shear failure ($P_{sm} > 0$) in both extensional and compressional stress regimes. In an isotropic stress regime, on the other hand, shear failure is unlikely. (The result for the isotropic stress regime is not shown in Figure 3, since in that case $P_{sm} < 0$, indicating no failure over the entire domain.) In the case of a compressional stress regime (Figure 3a), shear failure is most likely to be initiated in shallowly dipping (about 30° dipping) fractures at the interface between the permeable formation layers and an overlying caprock. In the case of an extensional stress regime (Figure 3b), shear failure is likely to occur in steeply dipping (about 60° dipping) fractures in the upper aquifer and in the overburden rock above the zone of increased fluid pressure.

Figures 4 and 5 present vertical profiles of fluid pressure as well as critical pressures for failure under the three different stress regimes. The vertical profile intersects the center of the model ($x = 0$), where, according to Figure 3, the potential for failure is the highest. Dashed lines show fluid pressure and critical failure pressures at initial conditions,

whereas solid lines indicate fluid pressure and critical pressures at 30 years. The results in Figures 4 and 5 show that critical fluid pressures for the onset of tensile and shear failure are not constant, but change during the injection.

Figure 4 shows that the biggest changes in critical pressure for tensile failure occur in the case of an extensional stress regime (Figures 4c). This is because injection-induced pore-elastic stress tends to develop in the horizontal direction, which is the direction of the minimum principal stress in that case. Thus, under the extensional stress regime, poroelastic stress increases the minimum (horizontal) principal stress and thereby tends to prevent tensile failure.

Figure 5 shows that the biggest changes in critical pressure for shear failure also occur in the case of an extensional stress regime (Figure 5c). In this case, injection-induced, poroelastic stress increases the horizontal minimum compressive stress, which acts as an additional confining stress that tends to increase the frictional shear strength of steeply dipping fractures.

Figure 5b shows that in the case of a compressional stress regime, there is only a slight reduction in critical pressure. In this case, injection-induced horizontal stresses act along the maximum principal stress direction and therefore have little impact on the minimum (vertical) principal stress. The noticeable change in critical pressure in Figure 5b is caused by an increase in the maximum (horizontal) stress, which tends to promote shearing along shallowly (about 30°) dipping fractures.

The simulation results also indicate that a high potential for failure exists adjacent to the ground surface, especially in the case of an extensional stress regime (Figure 4c and 5c). This finding may be partly an artifact from an assumed zero horizontal stress at the ground surface. At an injection site, small compressive stresses may exist even close to the ground surface and would prevent or reduce these near-surface effects. Moreover, if fractures were not considered completely cohesionless, even a small cohesion would tend to prevent shear failure in areas close to the ground surface. Nevertheless, upward migration of fluid pressure into the upper layers of the model domain induces additional strain on the overburden, which in general increases the likelihood of near-surface mechanical failure.

Figure 6 presents vertical profiles of the pressure margins for tensile and shear failure (Equations 8 and 9) at x=0, the injection point for the same three stress regimes. Three important observations can be made from the results shown in the figure. First, the potential for shear failure (that is, reactivation along pre-existing fractures) is higher than the potential for tensile failure for all three stress regimes. Consequently, shear failure would probably occur at a lower reservoir fluid pressure than tensile failure. Second, the highest potential for any kind of failure occurs in the upper parts of the pressurized CO_2 storage system, near the interface of the upper storage zone and the uppermost caprock (Caprock 3). Third, for the cases of isotropic and compressional stress regimes, shear failure may be initiated in the lower part of Caprock 3, but would not propagate through the entire caprock, which thus maintains sealing capacity in the upper parts. In the case

of an extensional stress regime, on the other hand, high potential for shear failure occurs throughout the CO_2 storage system and in preferentially steeply (about 60°) dipping fractures, with shear reactivation across the caprocks and in the overburden rock above the injection zone. Thus, at an injection site, it is important to analyze the mechanical changes that might occur in the upper layers above the injection zone.

Figures 7 and 8 present the evolution of effective stress paths (Figure 7) and pressure margin for the onset of shear failure (Figure 8), for two selected points in the system. Figures 7a and 8a show the evolution near the injection point (x = 0, z = -1,600 m), whereas Figures 7b and 8b show the evolution at Caprock 3, near its interface with brine-formation zone 3 (x = 0, z = -800 m). In Figure 7, the stress path is shown in σ'_1-σ'_3 space, for which the failure criterion in Equation (2) has been reformulated. For $S_0 = 0$ and $\varphi = 30°$, it can be shown that onset of shear failure would occur if $\sigma'_1 \geq 3\sigma'_3$ [16]. Figure 7 shows that the stress path crosses this limit after about 15 to 20 years near Caprock 3, under extensional and compressional stress regimes. Consistent with this, Figure 8 shows that the pressure margin for the onset of shear failure becomes positive after about 15 to 20 years. During a CO_2 injection operation, the evolution of fluid pressure as well as induced seismicity can be monitored and compared with simulated results to indicate when the injection rate would have to be decreased to avoid wide spread shear reactivation along pre-existing fractures and faults.

In addition to the cases presented in this paper, a compressional, strike-slip faulting stress regime could be analyzed. In a strike-slip faulting stress regime, the initial maximum and

minimum compressive stresses S_1 and S_3 are horizontal, whereas the intermediate stress, S_2, is vertical. In a strike-slip faulting stress regime, injection-induced poroelastic stress would tend to increase total stresses along both the directions of S_1 and S_3. This implies that, in general, injection-induced failure would probably be less likely under strike-slip compared to extensional and compressional stress regimes. However, the likelihood of mechanical failure, and the maximum sustainable injection pressure under any type of stress regime, very much depends on the magnitude and degree of anisotropy of the initial (pre-injection) stress field.

5 DISCUSSION

In this study, we conducted a coupled reservoir-geomechanical simulation to study the potential for tensile and shear failure associated with underground CO_2 injection in a multilayered geological system. We simulated a CO_2 storage system in which CO_2 was allowed to migrate upward through imperfections in the lower capping formations. In this section, we will compare our numerical results to those of more conventional and simplified analytical methods, and also to results for a single caprock system presented by Rutqvist and Tsang [3]. We will also discuss our results in terms of possible guidelines for estimation of maximum sustainable injection pressure at a geological CO_2 injection site.

If the site specific *in situ* stress field is not well known, it might be tempting to make a first-order estimate of sustainable injection pressure from the lithostatic stress, which could be estimated from the density of the overburden rock. In our simulations, the

injection pressure increased to a maximum of 25 MPa, which is about 71% of the lithostatic stress at 1,600 m depth. However, despite an injection pressure well below the lithostatic stress at the injection point, a high potential for failure occurred in the upper parts of the model. Moreover, shear failure (or shear slip) could occur in the two cases of initially anisotropic stress fields (compressional or extensional stress regimes). Thus, at a geological CO_2 injection site, it will not be sufficient to consider just the vertical lithostatic stress. The full three-dimensional stress field needs to be carefully characterized. Furthermore, to determine the maximum sustainable reservoir pressure, it we must investigate the potential for shear failure along pre-existing fractures, not just tensile fracturing.

At a geological CO_2 injection site, a more conventional analytical shear failure analysis may be performed based on planned injection pressure and a carefully characterized *in situ* stress field [4]. In an analytical shear failure analysis, the horizontal poroelastic stressing may be estimated for the idealized case of a thin, laterally extensive reservoir (i.e., the so-called passive basin) according to [19]:

$$\Delta\sigma_z = \alpha \frac{1-2\nu}{1-\nu} \Delta P \tag{10}$$

where α is Biot's coefficient and ν is Poisson's ratio. In this case, with $\alpha = 1$, $\nu = 0.25$, applying Equation (10) gives $\Delta\sigma_x = 0.67\Delta P$. That is, the total horizontal stress would increase by 0.67 of the fluid pressure change. Our results for the multilayered system show that the horizontal stress increases by a factor of only about 0.32 to 0.44 (Figure 9). This finding suggests that in this case, the thin, laterally extensive reservoir assumption in

the analytical solution is not valid. Thus, applying Equation (10) when conducting an analytical shear-failure analysis may overestimate the poroelastic stressing, which in turn could lead to an overestimation of the maximum sustainable injection pressure. As a remedy, alternative analytical or semi-analytical solutions (e.g., [20]) or a coupled reservoir-geomechanical numerical analysis may be applied to estimate the poroelastic stressing.

When comparing our simulation results for a faulted multilayered system to the results for an intact single caprock system by Rutqvist and Tsang [3], we can identify several important geomechanical issues related to the upward pressure migration in this system. First, if no upward leakage from Injection Zone 1 occurs, the assumption of a thin, laterally extensive reservoir is reasonably accurate, in which case, Equation (10) would provide a good estimate of poroelastic stressing within the injection zone. Thus, it is the upward migration of fluid pressure that results in the overestimated poroelastic stressing with Equation (10). Moreover, the upward migration of fluid pressure implies that the maximum sustainable injection pressure estimated at the depth of the injection point may not be the maximum sustainable pressure for the entire CO_2 storage system. Our analysis showed that in this particular scenario, the highest potential for tensile or shear failure occurred in the upper part of the system and in the overburden. If, on the other hand, no leakage were allowed, the fluid-pressure changes would be contained within Injection Zone 1 at depth, and the mechanical impact on the overburden would be much smaller. This shows that for a safety assessment, it is important to test and analyze different scenarios, such as the possibility of upward migration of fluid pressure.

At a geological CO_2 injection site, both analytical and more complex coupled reservoir-geomechanical failure analyses may be conducted, and may actually complement each other. As mentioned in the introduction, analytical techniques are indeed very useful for first-order estimates of the maximum sustainable CO_2 injection pressure, and for identification of the most critically oriented faults in the system. A first-order estimate of poroelastic stressing may be based on previous field interpretations [21, 22], or by the analytical and semi-analytical approaches described above [19, 20]. A coupled reservoir-geomechanical numerical modeling, on the other hand, might be suitable once more site-specific data on geometry and material properties are available. Moreover, coupled reservoir-geomechanical numerical modeling could be an integral part of site reservoir simulations and is a powerful tool for site-specific characterization, optimization, and performance confirmation.

Regardless of whether analytical or more complex coupled numerical techniques are utilized, our analysis shows that it is essential to have a good estimate of the three-dimensional *in situ* stress for design and performance assessment of an industrial CO_2 injection operation. Moreover, additional uncertainties in determining the maximum sustainable injection pressure arises from uncertainties in material properties, such as bulk modulus, Biot's coefficient, and shear strength of pre-existing fractures. Since the goal should be to prevent more significant failure and leakage from occurring, conservatism may be applied in selecting strength properties. However, the model

ultimately needs to be calibrated against site-specific field data, including passive seismic monitoring, before, during, and after active CO_2 injection.

6 CONCLUSIONS

We have conducted coupled reservoir-geomechanical simulations to study the potential for tensile and shear failure associated with underground CO_2 injection in a multilayered geological system. In this study, we focused on geomechanical stress changes resulting from upward migration of the CO_2 within the multilayered storage system, and how the initial stress regime affects the potential for inducing tensile and shear failure.

- The study shows that the potential for shear failure (reactivation along pre-existing fractures) is generally higher than the potential for tensile failure. Thus, at an injection site, shear failure along pre-existing fractures will probably occur earlier (at a lower injection pressure) than tensile failure.

- If upward migration of fluid pressure occurs in a multilayered CO_2 storage system, the estimation of the maximum sustainable injection pressure needs to consider the coupled fluid flow and geomechanical responses in the upper part of the system, where the potential for mechanical failure may be the highest.

- If injection-induced failure were initiated in a CO_2 storage system under a compressional stress regime, failure would preferentially occur along shallowly (about 30°) dipping fractures, but would be unlikely to propagate through the uppermost intact caprock, which could maintain its original sealing capacity.

- If injection-induced failure were initiated under an extensional stress regime, failure would preferentially occur along steeply (about 60°) dipping fractures within the storage zone, through caprocks, and in the overburden rock above the pressurized storage zone.

One important conclusion from this study is that the potential for mechanical failure, and the type and orientation of failure, depends to a large extent on the initial stress field (stress regime). Our analysis indicates that a compressional rather than extensional stress regime is favorable for limiting injection-induced mechanical failure and thereby preventing a significant breach of a geological CO_2 storage system. As such, the stress field should be much more carefully measured and monitored than is typical in the current practice for oil and gas explorations. Furthermore, the potential for mechanical failure should be analyzed for the entire region affected by mechanical stress changes, which is generally more extensive than the region of fluid pressure change at depth.

ACKNOWLEDGMENTS

We are grateful for internal reviews by Dr. Kenzi Karasaki and Dr. Dan Hawkes of Lawrence Berkeley National Laboratory, and external technical review by Professor Richard Hillis, University of Adelaide, Australia, which substantially improved this paper. This work was conducted with funding from the U.S. Environmental Protection Agency, Office of Water and Office of Air and Radiation, under an Interagency Agreement with the U.S. Department of Energy at the Lawrence Berkeley National Laboratory, and with funding from the Assistant Secretary for Fossile Energy, Office of

Coal and Power Systems, through the National Energy Technologies Laboratory, under Department of Energy Contract No. DE-AC02-05CH11231.

REFERENCES

[1] Poston SW, Berg RR. Overpressured gas reservoirs. Society of Petroleum Engineers, Richardson, Texas, 1997.

[2] Sibson RH. Brittle-failure controls on maximum sustainable overpressure in different tectonic stress regimes. Bull Am Assoc Petrol Geol 2003;87:901–908.

[3] Rutqvist J, Tsang C-F. Coupled hydromechanical effects of CO_2 injection. In: Tsang CF., Apps JA., editors. Underground Injection Science and Technology. Elsevier, 2005, pp. 649–679.

[4] Streit JE, Hillis RR. Estimating fault stability and sustainable fluid pressures for underground storage of CO_2 in porous rock. Energy 2004;29:1445–1456.

[5] Morris A, Ferril DA, Henderson DB. Slip tendency analysis and fault reactivation. Geology 1996;24:275–278.

[6] Wiprut D, Zoback MD. Fault reactivation and fluid flow along a previous dominant fault in the northern North Sea. Geology 2000;28:595–598.

[7] Mildren SD, Hillis RR, Kaldi J. Risk in brittle failure of caprock in the Otway Basin, Australia. AAPG Hedberg Research Conference, Barrossa Valley, South Australia, December1-5, 2002, pp. 108-110.

[8] Jones RM, Boult P, Hillis RR, Mildren SD, Kaldi J. Integrated hydrocarbon seal evaluation in the Penola Trough, Otway Basin, Australian Petroleum Production and Exploration Association Journal 2000;42:167–168.

[9] Rutqvist J, Tsang C-F. A study of caprock hydromechanical changes associated with CO_2 injection into a brine aquifer. Environmental Geology 2002;42:296–305.

[10] Rutqvist J, Wu YS, Tsang C-F, Bodvarsson G. A modeling approach for analysis of coupled multiphase fluid flow, heat transfer, and deformation in fractured porous Rock. Int J Rock Mech Min Sci 2002;39:429–442.

[11] Rutqvist J, Tsang C-F. TOUGH-FLAC: A numerical simulator for analysis of coupled thermal-hydrologic-mechanical processes in fractured and porous geological media under multiphase flow conditions. Proceedings of the TOUGH Symposium 2003, Lawrence Berkeley National Laboratory, Berkeley, May 12–14, 2003.

[12] Chadwick RA, Zweigel P, Gregersen U, Kirby GA, Holloway S, Johannessen PN. Geological reservoir characterization of a CO_2 storage site: The Utsira Sand, Sleipner, northern North Sea. Energy 2004;29:1371–1381.

[13] Corey AT. The interrelation between oil and gas relative permeabilities. Producers Monthly November 1954: p. 38-41.

[14] van Genuchten MT. A closed-form equation for predicting the hydraulic conductivity of unsaturated soils. Soil Sci Soc Am J 1980;44:892-898.

[15] Pruess K. ECO2N —A TOUGH2 Fluid Property Module for Mixtures of Water, NaCl, and CO_2. Lawrence Berkeley National Laboratory Report LBNL-57952. 2005. p. 58.

[16] Jaeger JC, Cook NGW. Fundamentals of Rock Mechanics. London: Chapman and Hall, 1979.

[17] Goodman RE. Introduction to Rock Mechanics. Second edition. New York: John Wiley & Sons, 1989.

[18] Barton CA, Zoback MD, Moos D. Fluid flow along potentially active faults in crystalline rock. Geology, 1995;23:683–686.

[19] Hawkes CD, McLellan PJ, and Bachu S. Geomechanical factors affecting geological storage of CO2 in depleted oil and gas reservoirs. J. Can. Pet. Technol., 2005;44:52–61.

[20] Segall P, Fitzgerald SD. A note on induced stress change in hydrocarbon and geothermal reservoirs. Tectonophysics, 1998; 289: 117–128.

[21] Segall P, Grasso JR, Mossop A, 1994. Poroelastic stressing and induced seismicity near the Lacq gas field, southwestern France. J. Geophys. Res., 1994; 99, B8: 15423–15438.

[22] Hillis RR. Pore pressure/stress coupling and its implications for seismicity. Exploratory Geophysics, 2000;31:448–454.

FIGURE CAPTIONS

Figure 1. Schematic of model geometry and boundary conditions of the multilayered CO_2 storage system.

Figure 2. Simulated coupled reservoir-geomechanical responses after 30 years of CO_2 injection into a multilayered and faulted system. (a) Spread of CO_2-rich fluid (solid-line contours) and changes in fluid pressure. (b) Fluid pressure induced changes in vertical (solid-line contours) and horizontal (dashed-line contours) effective stresses.

Figure 3. Calculated pressure margin for shear failure along pre-existing fractures after 30 years of CO_2 injection for (a) compressional stress regime with $S_x = 1.5S_z$, and (b) extensional stress regime with $S_x = 0.7S_z$. The region of high potential for hydraulic fracturing is also indicated in (b).

Figure 4. Vertical profiles (at x = 0) of fluid pressure and critical fluid pressure for hydraulic fracturing at initial conditions (dashed lines) and after 30 years of injection (solid lines) under (a) isotropic, (b) compressional, and (c) extensional stress regimes.

Figure 5. Vertical profiles (at x = 0) of fluid pressure and critical fluid pressure for shear failure along pre-existing fractures at initial conditions (dashed lines) and after 30 years of injection (solid lines) under (a) isotropic, (b) compressional, and (c) extensional stress regimes.

Figure 6. Vertical profiles (at x = 0) of pressure margins for onset of hydraulic fracturing (P_{fm}) and shear failure (P_{sm}) along pre-existing fractures and after 30 years of injection under (a) isotropic, (b) compressional, and (c) extensional stress regimes.

Figure 7. Effective principal stress path at (a) the bottom of the injection zone (x = 0, z = - 1600 m) and (b) in Caprock 3 at the interface with storage zone 3 (x = 0, z = - 800 m).

Figure 8. Time evolution of pressure margin for onset of shear failure at (a) the bottom of the injection zone (x = 0, z = - 1600 m) and (b) in Caprock 3 at the interface with storage zone 3 (x = 0, z = - 800 m).

Figure 9. Vertical profiles (at x = 0) of (a) change in fluid pressure, (b) change in total horizontal stress, and (c) poroelastic factor for fluid pressure induced changes in total horizontal stress after 30 years of injection.

Table 1. Material properties used in the basic coupled reservoir-geomechanical analysis.

Property	**Injection zone**	**Caprocks**	**Other storage zones and overburden**	**Base rock**	**Fractured zone (10 m wide)**
Young's modulus, E (GPa)	5	5	5	5	2.5
Poisson's ratio, ν (-)	0.25	0.25	0.25	0.25	0.25
Biot's coefficient, α (-)	1	1	1	1	1
Saturated rock density, ρ_s (kg/m^3)	2260	2260	2260	2260	2260
Effective porosity, ϕ (-)	0.1	0.01	0.1	0.01	0.1
Permeability, k, (m^2)	1×10^{-13}	1×10^{-19}	1×10^{-14}	1×10^{-17}	1×10^{-14}
Residual gas (CO_2) saturation (-)	0.05	0.05	0.05	0.05	0.05
Residual liquid saturation (-)	0.3	0.3	0.3	0.3	0.3
van Genuchten (1980), P_0 (kPa)	19.9	621	19.9	621	0.9
van Genuchten (1980) m (-)	0.457	0.457	0.457	0.457	0.457

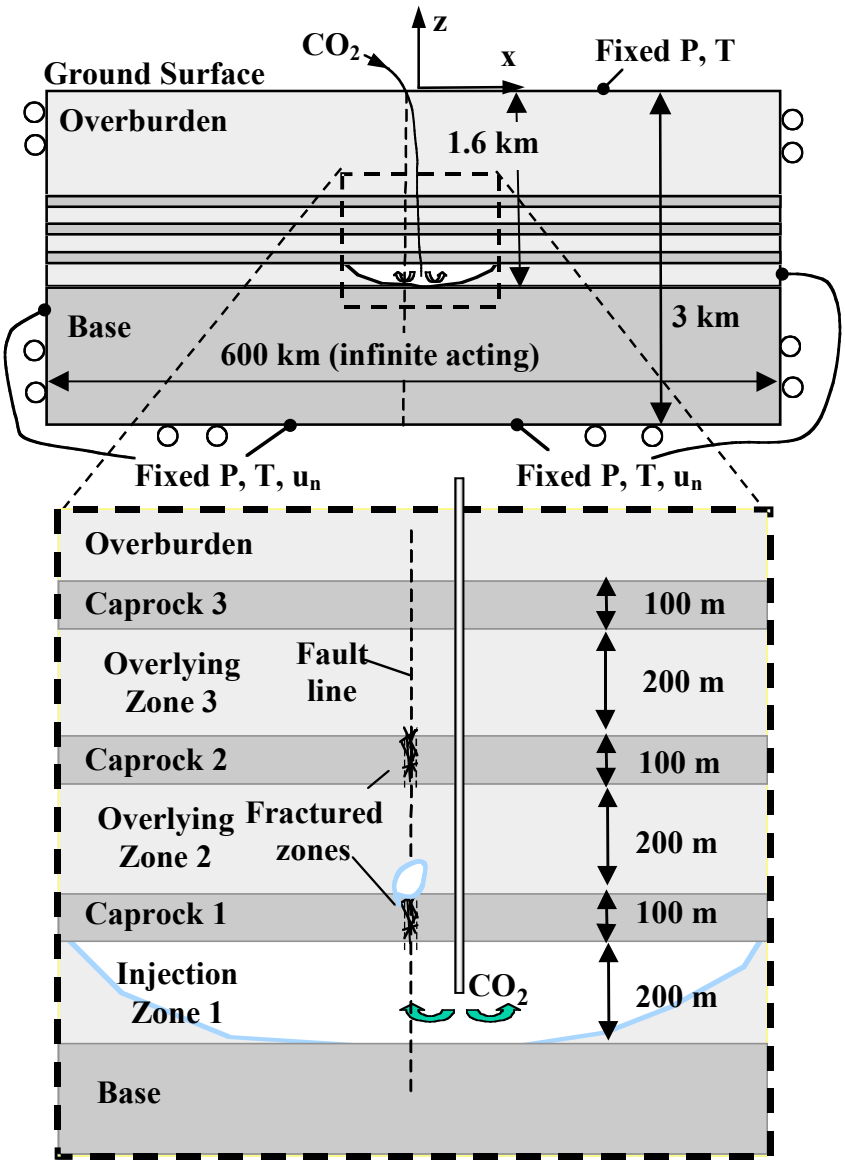

Figure 1. Schematic of model geometry and boundary conditions of the multilayered CO_2 storage system.

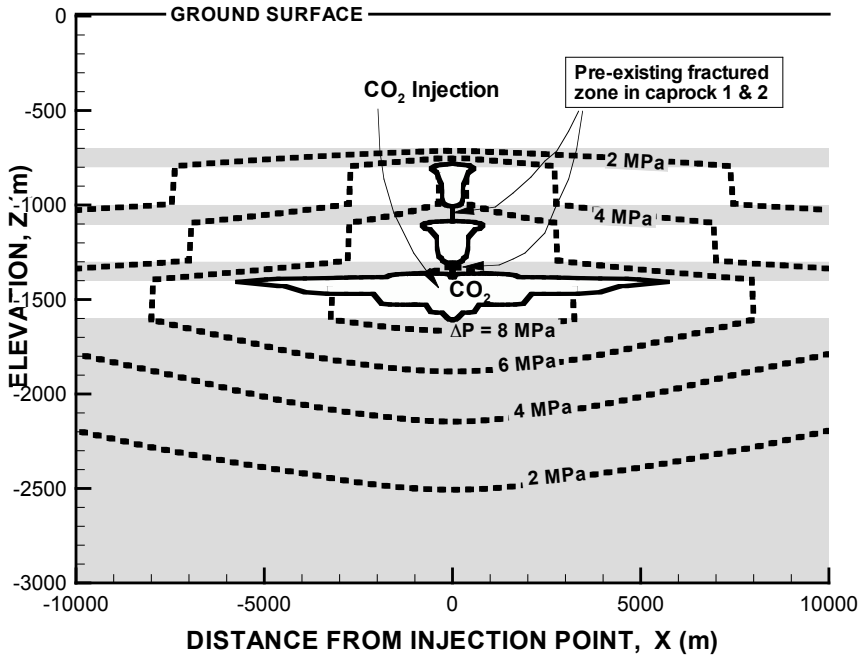

(a)

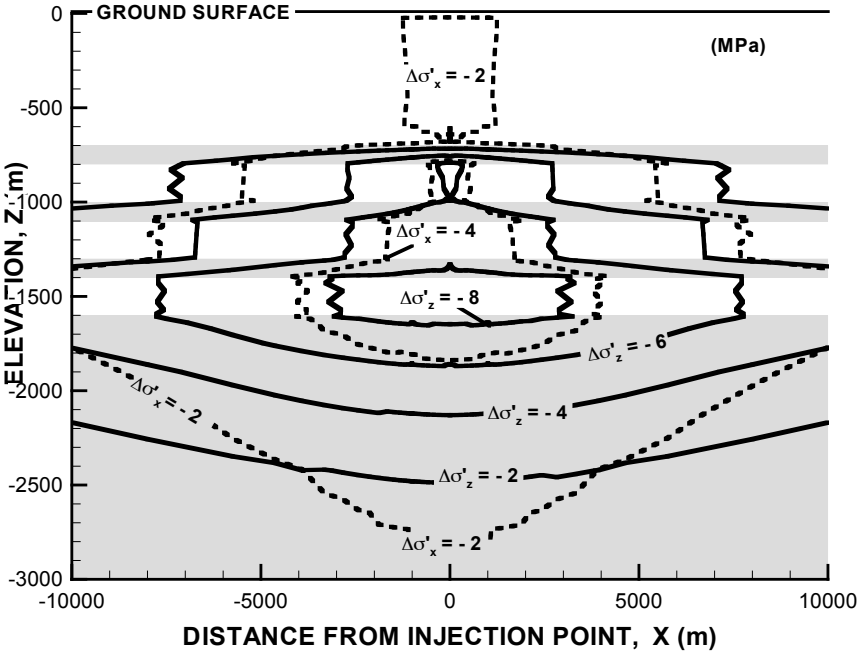

(b)

Figure 2. Simulated coupled reservoir-geomechanical responses after 30 years of CO_2 injection into a multilayered and faulted system. (a) Spread of CO_2-rich fluid (solid-line contours) and changes in fluid pressure. (b) Fluid pressure induced changes in vertical (solid-line contours) and horizontal (dashed-line contours) effective stresses.

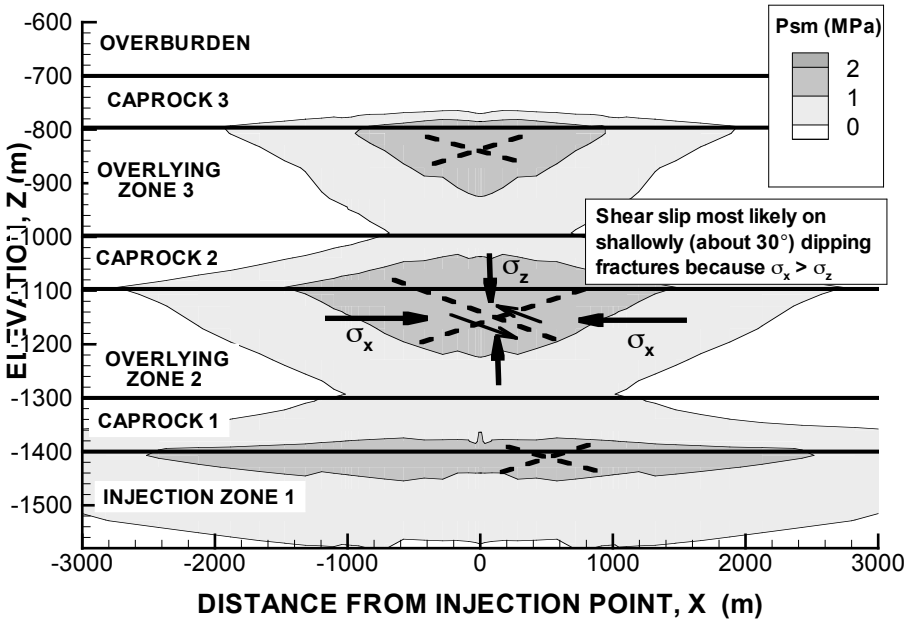

(a)

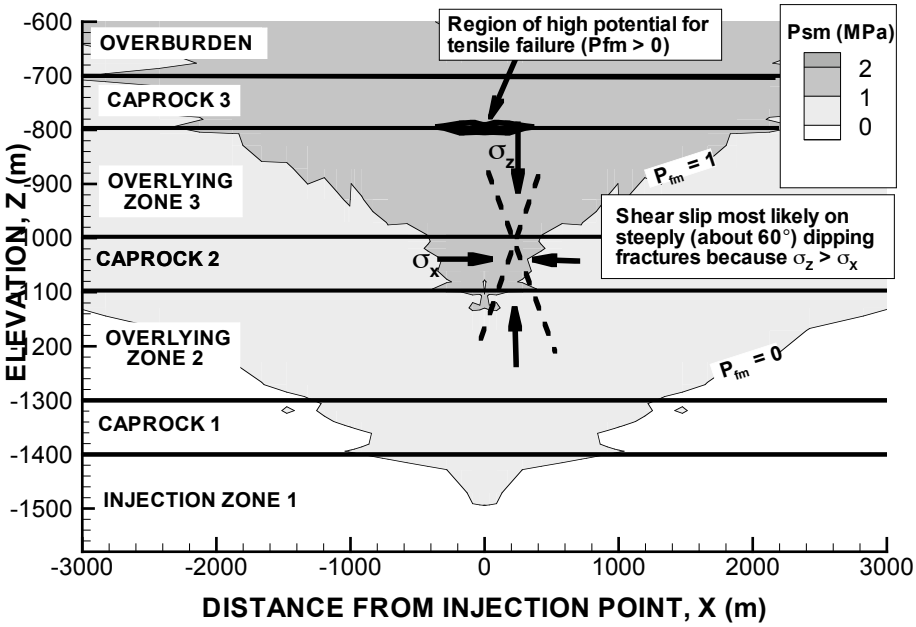

(b)

Figure 3. Calculated pressure margin for shear failure along pre-existing fractures after 30 years of CO_2 injection for (a) compressional stress regime with $S_x = 1.5S_z$, and (b) extensional stress regime with $S_x = 0.7S_z$. The region of high potential for hydraulic fracturing is also indicated in (b).

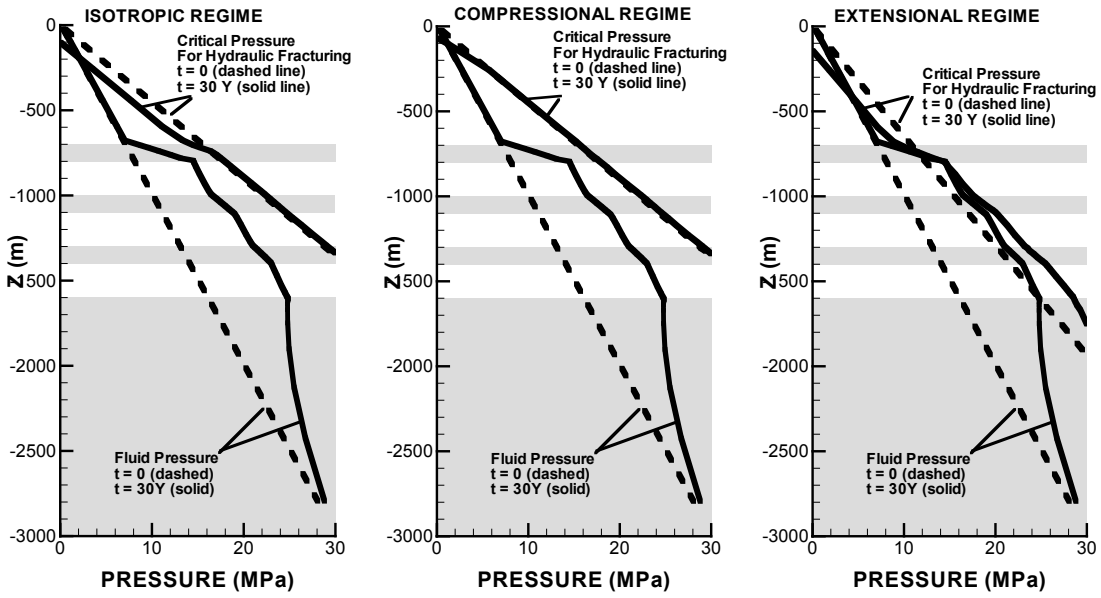

(a) (b) (c)

Figure 4. Vertical profiles (at x = 0) of fluid pressure and critical fluid pressure for hydraulic fracturing at initial conditions (dashed lines) and after 30 years of injection (solid lines) under (a) isotropic, (b) compressional, and (c) extensional stress regimes.

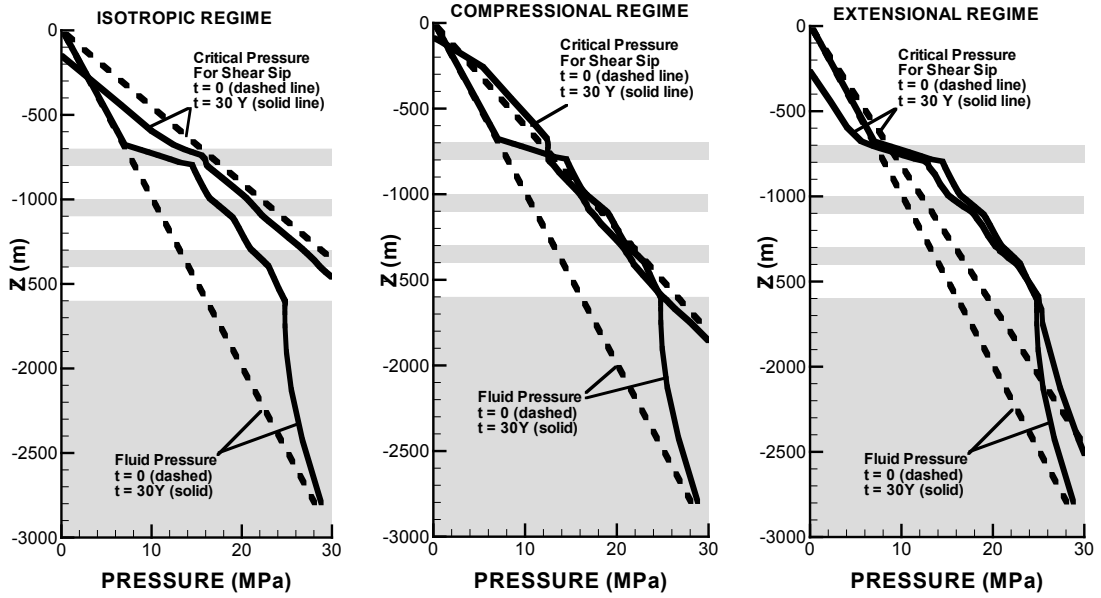

(a) (b) (c)

Figure 5. Vertical profiles (at x = 0) of fluid pressure and critical fluid pressure for shear failure along pre-existing fractures at initial conditions (dashed lines) and after 30 years of injection (solid lines) under (a) isotropic, (b) compressional, and (c) extensional stress regimes.

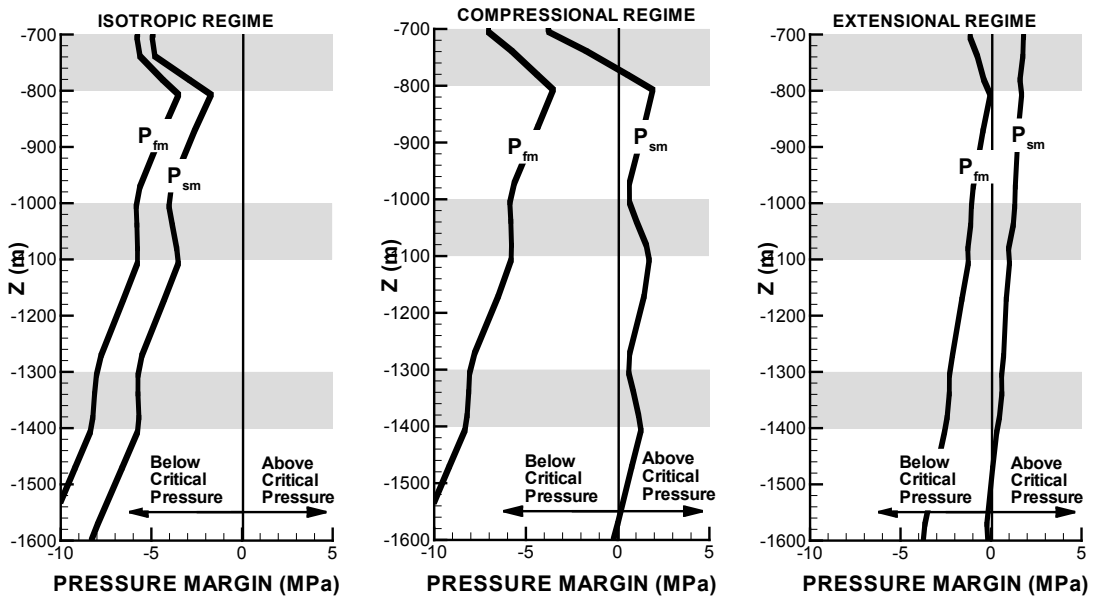

(a) (b) (c)

Figure 6. Vertical profiles (at x = 0) of pressure margins for onset of hydraulic fracturing (P_{fm}) and shear failure (P_{sm}) along pre-existing fractures and after 30 years of injection under (a) isotropic, (b) compressional, and (c) extensional stress regimes.

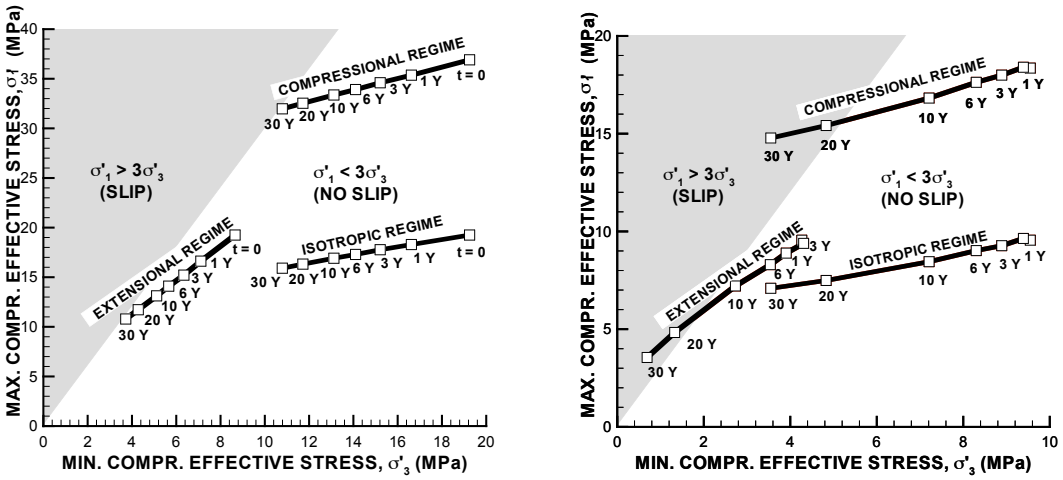

(a) (b)

Figure 7. Effective principal stress path at (a) the bottom of the injection zone (x = 0, z = - 1600 m) and (b) in Caprock 3 at the interface with storage zone 3 (x = 0, z = - 800 m).

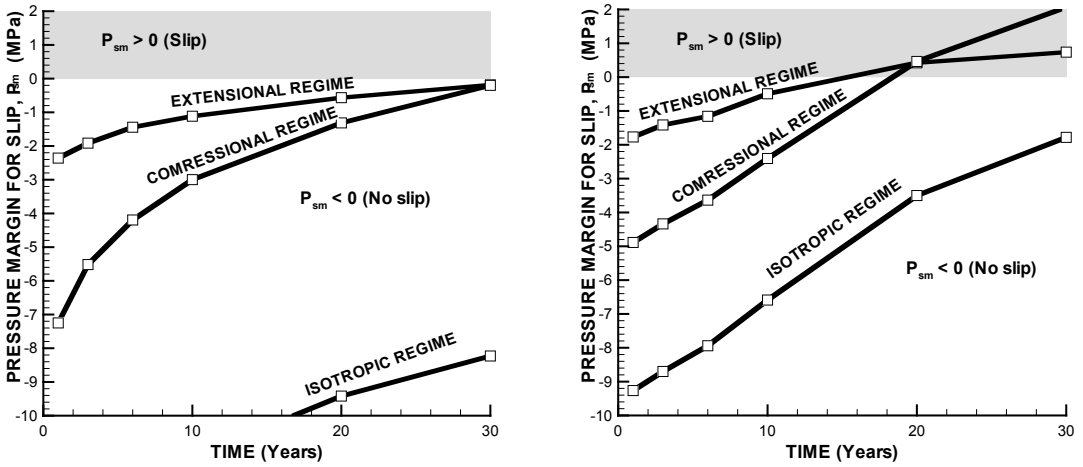

Figure 8. Time evolution of pressure margin for onset of shear failure at (a) the bottom of the injection zone (x = 0, z = - 1600 m) and (b) in Caprock 3 at the interface with storage zone 3 (x = 0, z = - 800 m).

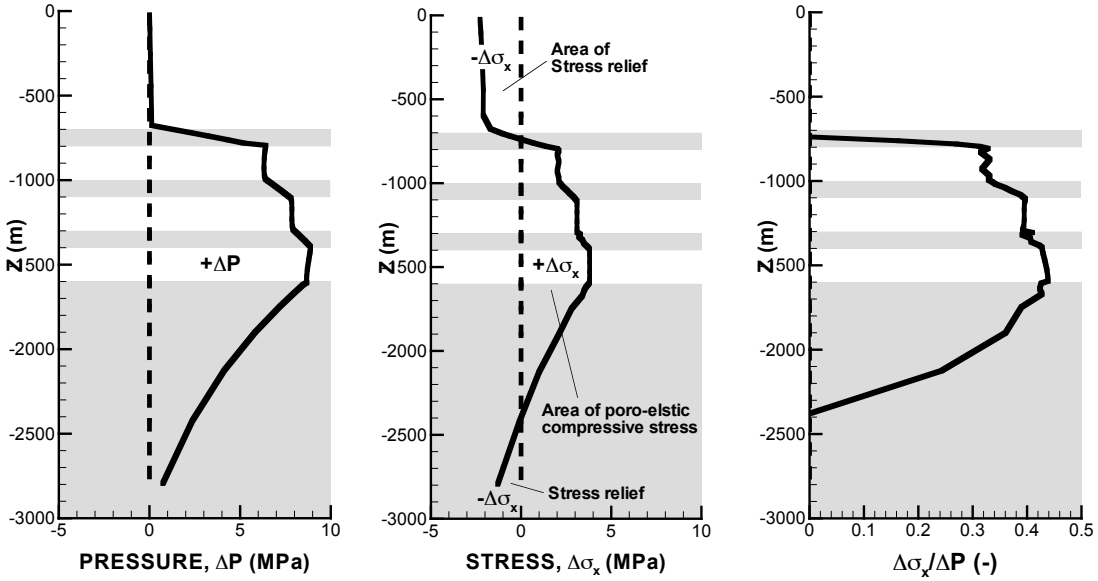

Figure 9. Vertical profiles (at x = 0) of (a) change in fluid pressure, (b) change in total horizontal stress, and (c) poroelastic factor for fluid pressure induced changes in total horizontal stress after 30 years of injection.